

Cloud fragmentation and proplyd-like features in H II regions imaged by HST¹

Orsola De Marco², C.R. O'Dell³, Pamela Gelfond⁴, R. H. Rubin^{5,6}, &
S.C.O. Glover²

ABSTRACT

We have analyzed HST ACS and WFPC2 new and archival images of eight H II regions to look for new proto-planetary disks (proplyds) similar to those found in the Orion Nebula. We find a wealth of features similar in size (though many are larger) to the bright cusps around the Orion Nebula proplyds. None of them, however, contains a definitive central star. From this, we deduce that the new cusps may not be proplyds, but instead are fragments of molecular cloud material. Out of *all* the features found in the eight H II regions examined, only one, an apparent edge-on silhouette in M 17, may have a central star. This feature might join the small number of *bona fide* proplyds found outside the Orion Nebula, in M 8, M 20 and possibly in M 16. In line with the results found recently by Smith et al. (2005), the paucity of proplyds outside the Orion Nebula, may be explained by their transient nature as well as by the specific environmental conditions under which they can be observed.

Several fragments are seen as dark silhouettes against a bright background. We have re-analyzed those found in IC 2944 by Reipurth et al. (2003) and found new, similar ones in M 16. None of these fragments contains a central star and we exclude that they are disks. Reipurth et al. (2003) concluded that the IC 2944 silhouettes are not star-forming. We argue here that their assumption of a constant optical depth for these fragments is not physical and that it is more likely that these fragments are star forming, a condition that is supported, although not proven, by their shapes and distributions. The process of cloud fragmentation *and* photo-evaporation produces a large number of small fragments, while the size hierarchy expected in a photo-evaporative environment would not favor small fragments. The size distributions observed will constrain any future theories of cloud fragmentation.

One bright micro-jet candidate is found in M 17 protruding from a large, limb-brightened fragment. A second, larger jet-like feature, similar in shape and size to a Herbig-Haro jet is found in Pismis 24. No central star appears to be associated with either of these jet candidates.

Subject headings: H II regions – planetary systems: protoplanetary disks – stars: formation – surveys

1. Introduction

The basic outlines of the processes of star formation are widely understood. We see the raw material for star formation in molecular clouds, and the end-product is seen in pre-main sequence and young massive stars on the main sequence. The hierarchical fragmentation of the molecular clouds and the formation of nascent stars has been elaborated from both ends of the process. At the beginning of the process one sees density concentrations within the molecular clouds, with sizes ranging down to the resolution of the methods for measuring them (Vannier et al. 2001). At the end of the process one sees young stellar objects (YSOs) such as the T Tauri stars and stars shrouded with varying amounts of obscuring opacity. A special class of YSO is the proplyds (a word

designed to replace the longer “PROto-PLANetarY Disks”; O’Dell et al. 1993), which are YSO’s found in or near an H II region, where the conditions for their observation are different from regions without a nearby ionizing star. The proplyds are easily visible because some are directly illuminated by the star(s) producing the H II region and hence have bright photo-ionized cusps facing the source of ionizing radiation. Other proplyds are not photo-ionized, but their dust component allows them to be seen in silhouette against the background emission of the H II region, while others demonstrate both properties. This means that it is possible to detail the nature of this class of YSO by direct imaging.

The early part of cloud fragmentation involves formation of large clumps which include the classical “Bok globules” (Bok & Reilly 1947), some of which contain YSO’s and others which may do so in the future. The physical size of such objects is about 0.35 parsecs (Clemens et al. 1991). The smallest fragmentation products will look like proplyds in that they will have outer portions smoothly sculpted by photo-evaporation of ionized material and cores that appear in silhouette. It is difficult to discern between a true proplyd, with an associated young star, and a compact fragment of similar appearance. The best studied region in the search for proplyds is the Orion Nebula with its embedded star cluster. The Orion Nebula Cluster is the closest cluster of stars containing an H II region (O’Dell 2001). There we see circumstellar material with diameters as large as 1730 AU (0.08 parsecs) and as small as the resolution of the Hubble Space

¹Based on observations made with the NASA/ESA *Hubble Space Telescope* (HST) obtained at the Space Telescope Science Institute, which is operated by the Association of Universities for Research in Astronomy (AURA), Inc., under NASA contract NAS5-26555.

²Astrophysics Department, American Museum of Natural History, Central Park West at 79th Street, New York, NY 10024
orsola@amnh.org

³Department of Physics and Astronomy, Vanderbilt University
Box 1807-B, Nashville, TN 37235
cr.odell@vanderbilt.edu

⁴Department of Physics, Yale University
217 Prospect Street, New Haven, CT 06511
pamela.gelfond@yale.edu

⁵NASA Ames Research Center
Moffett Field, CA 94035-1000
rubin@cygnus.arc.nasa.gov

⁶Orion Enterprises, M.S. 245-6, Moffett Field, CA 94035-1000

Telescope’s (HST) cameras (about 50 AU).

The search for proplyds in other H II regions is more difficult because of their greater distances. This makes it difficult to discriminate between a true proplyd, which by its classification as a YSO includes a nascent star, and fragmented portions of a molecular cloud that are subject to the same processes of illumination.

The search for proplyds has driven several studies (Brandner et al. 2000; Stapelfeldt et al. 1997; Stecklum et al. 1998; Bally et al. 1998; Smith et al. 2003), but results have been slow-coming. We know that in the case of the true proplyds, stars have formed and the circumstellar material is the remainder of the star’s placental material. Cloud fragments of larger size found in H II regions may or may not survive the hostile photo-evaporation environment long enough to produce a star. Several studies reported the detection of cloud fragments, some of which were tentatively interpreted as proplyd structures (e.g., Smith et al. 2003), while others were thought *not* to be forming stars (e.g., Reipurth et al. 2003). Never has a *bona fide* family of proplyds similar to those found in the Orion Nebula been found in another H II region.

The recent work of Smith et al. (2005) may provide the answer to the proplyds’ elusive nature. They found that the Orion Nebula proplyds are concentrated in the middle of the region, near the *very youngest* cluster stars, with ages of less than 0.5 Myr. Farther from the center, the number of proplyds diminishes, while the number of naked stars with low mass disks (detected via mid-IR emission) increases. They concluded that the typical proplyds

(star, disk and cusp) are very short-lived, so that after about 0.5 Myr only their descendants (stars with light disks) remain. If this interpretation is correct, it might explain the rarity of proplyds in other H II regions: to see proplyds we need nearby H II regions with very bright, extremely young stars.

In this investigation we increase the number of proplyd-like (and larger) fragments observed in H II regions. By determining the size hierarchy and morphological characteristics of these clumps of gas and dust in the context of those found in the literature, we provide new data to constrain theories of cloud fragmentation that may or may not produce stars.

In Section 2, we discuss the observations. In Section 3, we review the sample clusters’ properties from the literature; we survey the large scale Digital Sky Survey (DSS), and we classify interesting features within the Advanced Camera for Surveys (ACS) and Wide Field and Planetary Camera 2 (WFPC2) fields of view (FOVs). In Section 4, we compare the regions and interpret their features within the context of the Orion Nebula proplyds and proplyd-like features encountered elsewhere. We summarize in Section 5.

2. Observations

The observations presented in this paper were taken by HST ACS/WFI (FOV= 202×202 arcsec²) and WFPC2 (FOV= 150×150 arcsec²) Cycle 13 program GO9857 (PI: O. De Marco). In addition we have analyzed archival images from the ACS Early Release Observations of M 17 (program GO8992; PI: H. C. Ford) and the WFPC2 images of IC 2944 and M 16 acquired by programs GO7381

(PI: B. Reipurth) and GO9091 (PI: J. J. Hester), respectively. A list of the observations can be found in Table 1. The RA and Dec in Column 2 are the coordinates of the chip centers, measured in IRAF¹ (Tody 1986, 1993) using the DS9 (Joye & Mandel 2003) display, rather than from the image header. The position angle in Column 3 is the angle between the north direction and the y-axis of the ACS/WFC or WFPC2 chip assemblies. The ACS angle is obtained by adding 180 deg to the V3 angle from the image header, while the WFPC2 angle is obtained by adding 224.86 deg. All images were calibrated by the on-the-fly calibration pipeline. This was deemed sufficient for the purpose of the current investigation.

DSS images (POSS2/UKSTU, taken through the red filter, with a plate-scale of 1.01 arcsec/pix; Reid et al. 1991) of the H II regions, with an overlay of the HST apertures, are displayed in Figs. 1 to 8, while cluster and region parameters are listed in Table 2. The cluster coordinates are from the SIMBAD database². On these images we also mark the O stars. The WFPC2 apertures for the 6 visits of program GO9857 are also marked on the DSS images, although they are not presented in this paper due to the lack of interesting interstellar features.

¹IRAF is distributed by the National Optical Astronomy Observatories, which are operated by the Association of Universities for Research in Astronomy, Inc., under cooperative agreement with the National Science Foundation.

²The SIMBAD database, operated at CDS, Strasbourg, France.

3. The ionizing stars and cloud fragments within the H II regions

In this Section we review the observed H II regions' properties (Table 2) as well as their stellar content (Table 3). From the large-scale DSS images we determine the apparent size and general appearance of the H II regions as well as the distribution of O stars in relation to the position of the ACS or WFPC2 apertures (Figs. 1 to 8).

Feature numbers mentioned in the subsections below are those marked on the respective images (Figs. 9 to 14) and refer to the IDs in Table 4. One or two dimensions in AU are listed for every feature, where the distances in Table 2 have been used to convert angular into linear scales. The uncertainty on the measurements is $\sim 5\%$. Features discussed explicitly, but too small to be seen in Figs. 9 to 14 are also shown as thumbnails in Fig. 15³. All discrete features in the HST images smaller than $\sim 10\,000$ AU (most of which bear a resemblance to the Orion Nebula proplyds), are classified as either *cusps* or *silhouettes*. Cusps are limb-brightened, generally on one side. Silhouettes are not limb-brightened. Cusps and silhouettes can be attached to a large fragment or a ridge. When this is so they look like fingers or protuberances. We also list fragments larger than $10\,000$ AU in at least one direction (and call them *fragments* in Ta-

³While we do not attempt a precise morphological classification in this figure, the features are approximately sorted by type: attached cusps are followed by semi-attached ones, then detached ones. These are followed by tiny silhouettes called nodules larger circular silhouettes and an assortment of more complex fragments.

ble 4, although we also use the word in the text for features in general). These tend to be large and complex in shape with edges can be sharp, fuzzy, limb-brightened or a mix of the above.

3.1. NGC 6530

NGC 6530 is an extremely young open cluster in the Sgr OB1 association, located on the eastern edge of the Lagoon Nebula (M 8). The associated H II region has a roughly circular appearance with diameter ~ 18 pc (at a distance of 1.8 kpc; Sung et al. 2000). The walls of the cavity being excavated by the ionizing sources are visible to the north and south of the H II region and appear fairly sculpted with pillar-like and other structures (Fig. 1). There are some dark shapes in the DSS images with typical sizes of 0.015 pc, likely to be fragments of neutral material broken off from the walls by the UV radiation.

NGC 6530 contains three O stars immediately surrounding the ACS field of view (FOV; Table 3). They are Herschel 36, an O7.5 V star, 9 Sgr, an O4 V star and HD164816, an O9.5 III-IV star. There is also an O6.5 V+O6.5 binary (HD166052) about 19 arcmin (or ~ 10 pc at 1.8 kpc) eastward of the main group. Herschel 36 is thought to have a pre-main sequence companion (Allen 1986). The rest of the region (to the east of the O star cluster) is dominated by B stars. NGC 6530, and its population of pre-main sequence stars, has been intensively investigated by Sung et al. (2000), who also determined the distance to the cluster and its age (1.5 Myr with an age spread of 4 Myr).

In this region, Stecklum et al. (1998) have identified an ultra-compact H II re-

gion (G5.97-1.17), that they interpret as a circumstellar disk around a B0 star, which is being externally photo-evaporated by Herschel 36. The H α emission extends over 1080 AU, while the chord of the bow shock pointing toward Herschel 36 is ~ 600 AU. This is possibly one of the structures thus far discovered most similar to the Orion Nebula proplyds, whose cusp chords range in size between 50 and 440 AU (Bally et al. 2000). There are a few Orion Nebula proplyds with even larger sizes with two cusps having chords of 1700 AU (Henney & O’Dell 1999; Bally et al. 2005) at 430 pc (Warren & Hesser 1977).

We observed this region twice, the first time by aiming the ACS/WFC at a bright part of the region dominated by B stars (Fig. 1). The resulting ACS image appears bright and fairly smooth. Only on the eastern corner is there more extinction. No distinct features appear in this image and we do not discuss it further. Our second visit image was taken between the three O stars. In Fig. 9 we present a portion of the ACS image, where numerous short ridges are visible. Some of the ridges have protrusions and fingers pointing somewhere between the O4 V and O9.5 III-IV stars. The look of this region is very different from that of the others in that there are a lot of small bright features that give the region an “embossed” appearance.

There are 4 objects (#1-4) that are reminiscent of proplyd cusps, although their base might be attached to a ridge. The smallest and best defined of the four is #3. Its chord is 900 AU. The largest of them, #4, has a very rounded head and looks more like a protrusion from one of the faint ridges.

3.2. NGC 3324

This H II region is dominated by two O stars very close to one another, with spectral types O6.5 V(n) and O8.5 Vp (Table 3), located in the middle of a circular cavity with diameter 12 pc (at 3.0 kpc; Carraro et al. 2001; Fig. 2). They determined the possible presence of pre-main sequence stars and an age for the region of 2-3 Myr (which however could be an upper limit if the A0 I star HD92207 is not a member of the cluster). The cavity walls, as seen in the DSS image, are remarkably smooth. This is also the case at the higher resolution of the WFPC2 image, where only small protrusions can be noticed while the space immediately behind the ionization front is completely smooth with no features. The ACS image of this region, which included the two O stars, is very smooth too, with only a few areas where the opacity is higher. Given the lack of interesting features, we do not present either the ACS or the WFPC2 images of this region. As we will discuss later (Section 3.3), smooth ionization fronts do not appear to be associated with fragments.

3.3. NGC 2467

This H II region is about 8 pc (at 4.1 kpc; Feinstein & Vazquez 1989) in diameter (Fig. 3) and is dominated by one O6 Vn star (Table 3). There is also an O7 star 10 pc to the east, but its radiation would be much weaker than that of the O6 Vn star. The O6 Vn star is number 19 in the catalogue of Lodén (1966) who determined the cluster distance to be 1.355 kpc. However, from an analysis of the colors of 71 stars in the NGC 2467 region, Feinstein & Vazquez (1989) con-

cluded that the cluster is actually the superposition of two clusters with the earlier type stars being the farthest. This would position the O6 Vn star and its associated H II region (Sh 2-311) at a distance of 4.1 kpc. The only age estimate of the cluster was that of Lodén (1966, 7 Myr), which might be uncertain.

Our ACS image FOV is centered in the middle of the cavity and it includes the O6 Vn star (Fig. 10). Despite the large distance to this H II region, which makes it difficult to find any small-scale features (we estimated that 3 pixels, equivalent to 610 AU, are a minimum to discover a feature), the region is extremely rich in structure. Within the FOV we see several extremely sculpted limb-brightened ridges and many small and partly limb-brightened fragments. There are two ridged regions: a cluster of layered, structured ridges in the lower part of the ACS chip and a fainter, sculpted ridge running down the right side of the chip.

The extremely sculpted ridge cluster is very bright because of the diffuse emission from the ionization front. With no doubt, it is being sculpted by the O6 Vn star, since the large attached fragment (#40), as well as a number of thin fingers (e.g., #36, 38, 39) protrude toward it and are limb-brightened in that direction. On the top of fragment #40 there are two fingers, #41 and 42, with rounded tips and small, bright jets emanating from their tip and base, respectively (see also Section 4.4). To the right of the bright ridge cluster, where the brightness subsides, we see some cusps (#50-53) which appear to have once belonged to the ridge and might in fact have been the tips of thin fingers such as #24 or

#35, but have now been separated by the advance of the ionization front.

The ridge to the right is fainter (Fig 10). It is also better defined with a clear edge, beyond which the area is uniformly dark. The reason for the difference between this ridge and the bright layered ridges might be the viewing angle. The bright layered ridges could be farther away from us than the ionizing star. This would mean that the whole ridge surface (i.e., the main ionization front as well as what is behind the front) is illuminated from above. The faint ridge, on the other hand, could be slightly closer to us than the ionizing source, such that its body (the area of molecular cloud on the other side of the ionization front) is not illuminated and appears completely dark.

The faint ridge has a semi-detached large fragment (#26; oddly, this fragment appears to be brightened *also* from the north-east, but there is no cataloged ionizing source in that direction; the limb brightening could be the result of a complex projection effect). Similarly to fragment #40, fragment #26 has several protrusions (#28, 29) and even some smaller fragments (#27) which are breaking off from it. Some additional fragments appear to have been left behind by the advance of the ionization front (e.g., #16 and #22).

These isolated fragments are close to the line of sight to the O6 Vn star. Most of them are dimly limb-brightened (e.g., #13, #15), but some of them are not (e.g., #25). These fragments are not dissimilar to those in IC 2944 analyzed by Reipurth et al. (2003), but have the following differences: (i) These fragments are not embedded in a smooth medium, but in a medium

with variable patchy extinction. Most of them are limb-brightened, contrary to those in IC 2944. (ii) The NGC 2467 fragments are less dark than those in IC 1590 and their shapes include some very complex thin ones (e.g., #10), while in IC 2944 most fragments are very dark and very stocky. (iii) Many of these fragments contain cusp-like sub-units, which appear to be about to separate (#15 seems to be separating from #16, but it could also be that the two fragments share similar lines of sight). Some sub-units are seen nearby, but definitely separated (e.g., #13) from the larger fragments. The smallest of these protrusions (#12), with a chord of only 2.5 arcsec, or 1025 AU at 4.1 kpc is still attached to fragment #11. These rounded protrusions which are still attached or very close to the parent fragment are very similar in appearance to others that are definitely separated, such as #32, #33, #50 or #53. (iv) In NGC 2467 there are no isolated circular fragments, as is the case in IC 2944. (v) Last, in NGC 2467 the ionization front is relatively near the fragments; its proximity and appearance makes one suspect that the fragments have been left behind by the advance of the front. No such clear conclusion can be drawn for IC 2944.

3.4. Pismis 24

The extremely young cluster Pismis 24 was studied recently by Massey et al. (2001) who determined a high degree of co-evality for its numerous young O stars (0.7 Myr). As can be appreciated from Fig. 4, this is a very large H II region (~ 50 pc in diameter), although within it, there is a smaller and brighter H II region,

which is only about 2.5 pc in diameter. The ACS and WFC chips were placed on this region of intense emission known as G353.2+00.9 (Nr. 1404 in Paladini et al. 2003) to the south of the main H II region. Only one O star is embedded in the H II region, the others are grouped to the south.

The ionizing stars are concentrated in two distinct locations. The first and most important location is home to a very compact cluster of three O stars (O3 I, O3 II, and O7.5 V; Table 3) just off the southern edge of the ACS FOV. At the second location we find one isolated O6.5 V star located within the ACS FOV (Fig. 11). We will refer to these locations as ionization sources A and B, respectively. Off the edge of the ACS chip, in the same direction as the stars in location A, but farther away, are four additional O stars, which are less tightly grouped and might or not contribute significantly to the ionization of the features seen within the ACS FOV.

There is one long ridge extending from the top-left to the bottom-right of the ACS FOV (east to west; Fig. 11), which changes character as it runs along, from very sculpted to smooth. This ridge has one large and one smaller protrusion (#16 and #11), both similar to the large attached fragment in NGC 2467 (#40 there). Both protrusions end with a thin finger (#17 and #12). This ridge appears to be formed and ionized by photons from source A. A second ridge is layered on it (top-right corner in Fig. 11), but clearly limb-brightened by the star at location B. Facing the first ridge there is a third, smooth ridge (seen cutting the bottom left corner of Fig. 11), which appears to be limb-

brightened from the direction of the O6.5 V star in source B.

A group of several cusps are observed in this region (top-left corner of Fig. 11), some with peculiar shapes. Typically all chord sizes are close to 2000 AU (at 2.5 kpc) although the smallest cusp (#8) has a chord length of 500 AU. All of the cusps are between the first and second ridge. Some of them (#1, #2, #7, #8 and #9) point toward ionizing location A, while others (#5 and #6) point somewhere between A and B. Another cusp (#4) in the same group is a very long (7700 AU) bacterium-shaped object, pointing toward source B, with both sides of its long body limb-brightened. A second source (#3) is larger (12 000x15 000 AU) and has the shape of an upside down heart, with very smooth, limb-brightened edges which again appear to be illuminated from both sides. We call this a *cusp* because of its smooth, limb-brightened edges and its location close to other cusps, but we note that its size is closer to a *fragment* than a *cusp*.

Near the second ridge we see one of the strangest objects yet encountered: a circular object (#18), seen in silhouette and not limb-brightened, with a dark oval core of size 2625x2125 AU, embedded, but not centered, in an oval, grey halo 5380x4000 AU.

Finally, the ionized area between the two smooth ridges (between the lower part of ridge one and ridge three; lower left corner of Fig. 11) is fairly smooth and devoid of features, reinforcing the conclusion already drawn for NGC 3324 (Section 3.2) that fragments and cusps are seen only in association with very sculpted ridges.

3.5. IC 1590

IC 1590 is an H II region with an approximate size of 21 pc at 2.94 kpc (Guetter & Turner 1997). On the eastern side of the DSS image (Fig. 5) we find the ionization front eating into the molecular cloud. Several protrusions are seen extending out from this ridge. Our WFPC2 image is centered on one such trunk, but the low SNR prevented us from being able to study it in detail. The stellar content of this region consists of a rich and compact cluster comprising a few O stars with spectral types between O6.5 V and O9 V, possibly all in binary and even triple systems (Guetter & Turner 1997; Table 3).

Dark fragments can be seen in the DSS image scattered around the ionized region. Within the FOV of the ACS chip, which includes the ionizing sources, we see only one such fragment (#1), very similar to the “Thackeray globules” (Thackeray 1950) studied by Reipurth et al. (2003). Unfortunately this image is underexposed and we can therefore only distinguish two smaller fragments (#3 and #4) that appear to have broken off from the main fragment. These two fragments have sizes of 8500 AU and 6800x20 000 AU, respectively and are therefore comparable to fragments breaking off the ridge in NGC 2467 (e.g., #27 there).

Although these fragments are not very close to the eastern ionization front, they are close to an area of high extinction covering the south corner of the ACS chip. This extinction is likely due to neutral material in the foreground on the near side of the region. Whether the fragment on the ACS chip has broken off from the ridge on the east side of the DSS image, or from

another, hidden ionization front is hard to say. We note that the presence of a large fragment seen in silhouette against the ionizing sources and not obviously close to a ionization front, is similar to the situation encountered in IC 2944 (Reipurth et al. 2003) and M 16 (Section 3.7).

3.6. IC 2944

IC 2944 is a large faint H II region about 28 pc in diameter (at a distance of 1.8 kpc; Ardeberg & Maurice 1980). It is ionized by a cluster of nine O6-O9.5 V stars which was studied by Walborn (1987), who concluded that the stars belong to one cluster, rather than being a chance superposition of more than one cluster. He determined a distance to the cluster of 2.0 kpc based on the stellar types. The cluster’s age is 7 Myr (Dutra et al. 2003; Bica et al. 2003). This is the oldest cluster in our sample.

Reipurth et al. (1997) studied the “Thackeray’s globules” in this region from ground-based imaging. They adopted a distance of 1.8 kpc, previously obtained by Ardeberg & Maurice (1980) from nebular kinematic arguments. Given the similarity of the two distance estimates and the fact that we will make extensive comparison with the study of Reipurth et al. (1997), we will adopt their value. From the lack of CO emission, Reipurth et al. (1997) concluded that the globules are not star-forming. They are instead transient fragments of neutral gas and dust that broke off from the main walls. The dynamical lifetimes of the clumps, of the order of 1 Myr, obtained from kinematic arguments, agree with transient clump lifetimes predicted from magnetized hydrodynamical models of Vázquez-Semadeni et al. (2005). (These

models do not include the effects of radiation, which is likely to be an important factor in the destruction of the clumps. However, we know of no model predictions which does include the effects of radiation, so this is as good a comparison with theory as we can make at present, although one could suggest that the model timescales are only an upper limit).

We have re-analyzed the WFPC2 image of Reipurth et. al (2003). In Table 4 we list the fragments using their numbering system; we precede their numbers by an “R” to separate those fragments identified by them from a few that they did not list. We do not present the WFPC2 image, since it can be seen in that paper. The fragments are seen silhouetted (and sometime dimly limb-brightened) against a bright uniform background. The O stars in the region are scattered to the north, north-west and south of the FOV. The closest star is an O7 III star just south of the FOV. The next closest star is an O8 V star 0.7 pc to the south-west. All the other stars are farther (Fig. 6). The fragments range in shape from complex to perfectly circular. The largest fragment (#R1; 30 000x50 000 AU) is very complex and structured, with dozens of appendages. This can be compared to fragments #1 in IC 1590 and #4 in M 16. Other fragments are smaller but still have irregular shapes (#R2, #R30/1; 18 000x10 000 AU and 6000x3200 AU, respectively; Fig. 15). Smaller fragments have elongated or rounded, though slightly asymmetric shapes (e.g., #R37 and #R32; 1500x3200 AU and 2200 AU, respectively; Fig. 15). Finally, the smallest fragments are either perfectly circular (#R33 or #R27; 1800 AU and 1000 AU, respec-

tively), or too small to resolve their shape (e.g., #R40A, B and C [Fig. 15] and #R41; the first three have a diameter of <500 AU, while the last is 540 AU wide).

3.7. M 16

The stellar content of M 16 (also known as NGC 6611 or the Eagle Nebula) was investigated by Belikov et al. (1999) and Belikov et al. (2000) who determined the distance to the cluster to be 2.14 kpc and its age to be 6 Myr with a similar age spread. The bright H II region has an approximate diameter of 18 pc and it is very rich in O stars: at least nine O stars with spectral types between O4 and O9.5 are found in the region (Table 3).

M 16 was thoroughly investigated by Hester et al. (1996). They observed the region near the large dusty “elephant trunks” (a set of three dusty pillars; their FOV is marked in Fig. 7) and concluded that the several cusps near the “elephant trunks” are star-forming nodules left behind by the ionization front eating into the molecular cloud. We have looked at a WFPC2 archival image of a slightly different part of the region. Our FOV (placed only a few arcminutes to the north-west; Fig. 13) contains a large fragment (#4) similar to a typical “Thackeray globule” with a very long, round-tipped protrusion (#7), and two perfectly circular fragments (#1 and #2; 750 AU and 1500 AU in diameter, respectively; Figs. 13 and 15) similar to those encountered in IC 2944.

3.8. M 17

M 17 is one of the brightest H II regions in the galaxy. Hanson et al. (1997) studied its massive star content and determined

the presence of a large number of massive YSOs and an age for the cluster of only 1 Myr. They also determined the distance to the region to be 1.3 kpc.

The region within the ACS FOV is very rich, with diffuse features not seen in the other images. In Fig. 14 we show a portion of the FOV with two large, but oddly very smooth, fragments (#4 and #5) which might be attached to a ridge outside the FOV. There are also three classical cusps in this image (#3, #9 and #10), with chords of 720, 320 and 650 AU, respectively. Cusp #9 is the smallest cusp detected outside the Orion Nebula and is close to the 3-pixel detection limit for a feature in this region. There is also a most curious long fragment (#6) with a limb-brightened cusp facing one of the hottest ionizing sources. From it protrudes a bright straight jet (see also Fig. 18 and Section 4.4). The other side of the fragment consists of a very thin tail. Just north of the tail is a small boomerang-shaped fragment seen in silhouette (#8). There is one circular silhouette in this region (#7; not included within the FOV of Fig. 14 but shown in Fig. 17) in the middle of an area of extremely bright emission. It also appears to have a halo, similar to silhouette #18 in Pismis 24. The inner, darkest part of the feature is shaped like a boomerang (Fig. 17).

In M 17, we also find the only fragment (#12; not included within the FOV of Fig. 14) with a possible central star. This silhouette looks like an edge-on proplyd disk. In Fig. 16, we show four images of the same region of sky in four different filters. Around one of the stars, we see what could be an edge-on dusty disk, 1170 AU in diameter and 195 AU thick. The star at its

center is a faint red star. The object most similar to this, is Orion 114-426, where an 860-AU edge-on disk partly obscures a central star (McCaughrean & O’Dell 1996). We notice that the central star in our fragment is not exactly centered. This however could be similar to the situation encountered in HH513 (Orion 165-235) where the star embedded in the disk is offset from the disk’s center, and it is thought to be the companion of a hard-to-detect central star (Bally et al. 2000). An alternative explanation was pointed out by the Referee: what is seen as the central star could also be reflection of stellar light from the inner rim of the disk. This would appear off-center if the disk’s inclination angle was not exactly 90 degrees.

4. Discussion

Below, we group some of the most interesting characteristics of the features found in the H II regions and compare them across regions and with results from the literature.

4.1. The shape, size and limb-brightening properties of the proplyd-like fragments

With the observation of a large number of H II regions one could hope to find proplyd-like fragments bridging the gap between the *bona fide* Orion Nebula proplyds (where a star is surrounded by a dark disk seen in silhouette, often embedded in a bright, tear-shaped cusp) and the bright, similarly tear-shaped cusps with no central stars, found in other regions.

In order to compare the fragment sizes and size distributions found in different re-

gions, we have converted the angular sizes to linear sizes (in AU) using the distance estimates from Table 2 and calculated the effective radius of each fragment. The effective radius is defined by Reipurth et al. (2003) as the square root of the fragment’s area. In order to compare with their results we have maintained the same definition. If the fragment is rounded and is characterized by only one measurement in Table 4, we assume that fragment to be a circle and the measurement to be the diameter. If the fragment has a short and a long measurement in Table 4, we assume it is a rectangle. In this way some areas are overestimated, in particular for intermediate size, complex fragments such as some of those in NGC 2467. However, the smallest fragments, which are almost always rounded, are well represented by our calculation. Overall, our approximation has no bearing on the conclusions.

Reipurth et al. (2003) carried out a similar analysis and concluded that if *photo-evaporation* was the only process determining the fragment size distribution, there should be fewer small fragments. They therefore suggested that *fragmentation* produces small fragments at a high rate. Their size distribution has two peaks, one at less than 1 arcsec (<1800 AU) and one at 1.5 arcsec (2700 AU). We reproduced their histogram using our measurements (Fig. 19; second-to-last panel). There, we see a distribution with a broad peak centered at ~ 1000 AU, extending between 300 and 5000 AU. We therefore confirm the presence of a large number of objects smaller than 1800 AU but do not resolve the peak at size 2700 AU (possibly because of our coarser measuring method).

NGC 2467 has a distribution peaked at larger sizes than IC 2944 with two peaks at sizes 3200 and 8000 AU (or one peak at ~ 5000 AU). The smallest detected size (800 AU) is larger than in IC 2944, probably because NGC 2467 is much farther (4.1 vs. 1.3 kpc; 3 pixels = ~ 600 AU). Pismis 24 has fewer fragments and the smallest fragments, ~ 790 AU across, are quite a bit larger than the 3-pixel detectability limit at 2.5 kpc (~ 370 AU). The largest fragments in Pismis 24 (which are cusps) are similar in size to those in IC 2944 (which are silhouettes). Finally, although we cannot assess the fragment size distributions for the other H II regions, we note that M 17 has fragments as small as those in IC 2944, although they are cusps rather than silhouettes. We also note that cusp #9, found very close to cusp #10 in M 17 (M 17-9 in Fig. 15), with a chord size of only ~ 320 AU, is the smallest cusp ever detected outside the Orion Nebula.

Proplyd cusps observed within the Orion Nebula are the bright ionization fronts where the external radiation field ionizes the material photo-evaporated from the circumstellar disks. Cusps found elsewhere, in particular where no star is present, might be lumps of dusty gas externally photoionized by the nearby O stars, either on the way to forming a star or just transient.

In Table 5, we summarize the size ranges of bright cusps and dark silhouettes from the literature alongside those determined here. For the Orion Nebula, we have taken as representative the proplyds in Fig. 7 of Bally et al. (2000). The smallest bright cusp found there, 179-353, has a chord of ~ 50 AU. The largest, 206-446, has a

chord of 440 AU. However, Orion Nebula cusp chords can be as large as 1700 AU, as are those of proplyds 244-440 (Henney & O'Dell 1999) and 181-826 (Bally et al. 2005). For the Orion Nebula silhouette disks the range is 65-800 AU (where at the small end we find 182-332, while at the large end we find 114-426). We use these values as fiducial marks for our comparison.

Outside the Orion Nebula, the only objects that can be classified as possibly *bona fide* disks, because of the presence of a central star, are the disk found in M 20 (Table 5; Yusef-Zadeh et al. 2005), the cusp found in M 8 (Table 5; Stecklum et al. 1998), some cusps with central stars found in M 16 (Table 5; Hester et al. 1996), as well as the edge-on disk found by us in M 17 (but see section 3.8 for our reservations). The dark, perfectly circular silhouettes found in M 16 and IC 2944, and the circular silhouette with a halo found in Pismis 24 do not contain a central star.

Some of the cusps in Pismis 24 and M 17 have sizes small enough (750 AU and 315-845 AU, respectively) to compare with some of the cusps in the Orion Nebula, but have no central stars. As such, until the central star is detected, they remain in the same class as the larger (chords >800 AU) starless cusps, although their sizes can be similar to the sizes of the Orion Nebula proplyds and, as such, they are closer to *bona fide* proplyds than, for instance, the fragments found in Carina (Smith et al. 2003). The large cusps with no central star found in Carina by Smith et al. (2003) and in NGC 6303 by Brandner et al. (2000) are likely to be fragments of molecular cloud. This is also likely to be the case for the

large-to-intermediate size cusps found in NGC 2467, although, due to the higher resolution of the NGC 2467 observations, we can detect cusps with smaller sizes than those detected by Smith et al. (2003) and Brandner et al. (2000).

Finally, we compare the starless circular silhouettes found in IC 2944 and M 16 with the tear-shaped cusps found within this work and elsewhere. These cusps and silhouettes can have similar sizes. We therefore suggest that they are all self-gravitating fragments of molecular cloud: they acquire a tear-drop shape and a photo-ionized limb when embedded in the radiation field, but lose the bright limb and acquire a more spherical shape when shielded from the direct radiation (this is confirmed by models by Henney & O'Dell 1999).

The more important question, in the absence of a central star, is whether star formation is taking place in these cusps and silhouettes.

4.2. Are the circular silhouettes and the tear-shaped cusps star-forming?

The circular appearance of a number of silhouette fragments and the tear shape of cusps in our sample could be easily explained if these objects are self-gravitating and are in the process of collapsing to form stars. This is also an implicit assumption of the claim made in Section 4.1 that circular silhouettes acquire their spherical shape when shielded from the direct ionizing radiation which would otherwise shape them into tear-drops. Reipurth et al. (2003), however, measured a rather low optical depth across the face of some of their cir-

cular silhouettes, and deduced that they are not star forming. The jury appears therefore to be still out on the star-forming properties of these fragments and their relationship to *bona fide* proplyds.

Using the same optical depth argument, we compared the characteristic sizes of the circular silhouette fragments in IC 2944 and M 16 with the gravitational stability length scale, or Jeans length (Jeans 1902), for gas with the same density and temperature as the globules. Using the H α optical depth determined by Reipurth et al. (2003) ($\tau \sim 0.1$ – 1), we constrain the globules' total hydrogen column density along the line of sight to be $N_{\text{H}} = 10^{20}$ – 10^{21} cm $^{-2}$. If we assume that the characteristic size of a given globule along the line of sight, L , is similar to its observed size in the plane of the sky, or in other words that our circular globules are indeed approximately spherical, then we can use this to constrain the mean volume density of the gas:

$$\bar{n}_{\text{gl}} \simeq 6.7 \times 10^3 \left(\frac{\tau}{0.1} \right) \left(\frac{L}{1000 \text{ AU}} \right)^{-1} \text{ cm}^{-3}. \quad (1)$$

If the density distribution in a typical globule is approximately uniform, then the Jeans length within it will be:

$$L_{\text{J}} = 8.3 \times 10^4 \left(\frac{T}{10 \text{ K}} \right)^{1/2} \left(\frac{\tau}{0.1} \right)^{-1/2} \left(\frac{L}{1000 \text{ AU}} \right)^{1/2} \text{ AU}, \quad (2)$$

where T is the gas temperature. Even for $\tau = 1$, this gives a value for L_{J} that is at least an order of magnitude larger than the size of a typical spherical globule. Also, while it would be possible in principle to reduce L_{J} by reducing the gas temperature T , it does not appear plausible to have $T \ll 10$ K; instead, we would actu-

ally expect that $T > 10$ K, due to photoelectric heating of the gas by the diffuse nebular emission. This line of reasoning would therefore lead to the same conclusion of Reipurth et al. (2003), namely that the small spherical silhouettes seen in IC 2944 and M 16 are not gravitationally bound.

This argument may contain a basic flaw because of an assumption made. The implicit assumption in both the Reipurth et al. (2003) and the Jeans length arguments is that the globules have relatively flat internal density distributions. This assumption is made because of the flat brightness distribution within the fragments. It is however highly unlikely that the densities within the fragments are constant: unless the objects have the same physical thickness across their faces, then a constant optical depth would mean that (for a spherical object) the spatial density decreases towards the middle owing to the path-length increasing. The most likely explanation is that the optical depth flattening out at about unity (and being limited to about unity) is due to filling-in of the light by the finite diffraction pattern of the telescope-camera. The images of the fragments are surrounded by very bright nebulosity and this tends to fill-in the central regions, thus limiting the *apparent* optical depth and leading to underestimates of the spatial density (McCaughrean & O'Dell 1996). If instead the globules have strongly peaked central density distributions, then their inner regions will be more strongly bound than this simple argument suggests and indeed might be in the process of making stars.

Besides their shapes, there is another ar-

gument in favor of the circular silhouettes and cusps being in the process of making stars. Cusps are found only in proximity to the cavity walls, indicating that they might have been recently freed from the molecular cloud walls by the advance of the ionization front and indicating in turn that they are considerably denser than the molecular cloud mix. Based on this we would argue, although cannot prove, that these tear-shaped cusps might well be self gravitating and star-forming.

This conclusion is also in line with the results of Smith et al. (2005) who found the proplyds in the Orion Nebula only in close proximity to the youngest hot stars, while farther from these stars they only detect the proplyd descendants, mid-IR emitters interpreted as stars with feebler disks. In this scenario, stars of all masses are forming in the molecular cloud. What we see, however, is dictated by the early evolution of the most massive of them. True proplyds should be common, *but* they are only seen if they are illuminated by a nearby, very hot star, *even if* they do not last long in close proximity to such intense radiation. When the proplyd disk has been sufficiently evaporated by the hot stars, the proplyd appearance vanishes (it loses its bright skin), although its central star still retains the thinned out disk and is detected as a mid-IR emitter, near what has become a slightly older O star. In parallel with the emergence and demise of proplyds, the O star ionization front progressively frees star-forming clumps, ionizing their outer parts, shaping them into tear-drops and initiating their evaporation. As a result, these cusp-like objects do not last long, which explains why we see them only near

the cavity walls, where they have been recently freed. The star(s) made in these clumps eventually emerge from their placental material, but might never be seen as proplyds because they are not sufficiently close to the ionizing source(s).

With hindsight, the Referee's suggestion that we should have observed H II regions containing groups of pre-main sequence low-mass stars in close proximity to O stars, is right. However, this further constraint would have resulted in overall larger distances to our H II region sample, making the detection of small features harder still.

4.3. Smooth ionization fronts

In some regions, namely NGC 3324 and parts of Pismis 24 the ionization front is smooth. This means that there are no protrusions or broken fragments of any size. Is this lack of features associated with the type and age of ionizing stars and their geometric distribution? Or is it a characteristic of the molecular cloud itself? It looks like some molecular clouds, for some reason, neither fragment nor contain small clumps waiting in the molecular cloud to be freed by the passage of the ionization front. This characteristic does not appear to be related to age since although NGC 3324 is young, so is M 17 which has a variety of features. Also, Pismis 24 has both sculpted (with nearby fragments) and smooth (with no nearby fragments) walls, confirming that the smoothness of the wall has nothing to do with the age of the region. It appears more likely at this stage that the lack of fragments is due to the nature of the molecular cloud itself.

4.4. Jets

Four jet-like structures have been observed in the H II regions (Fig. 18). Two of them (#14 in Pismis 24 and #6 in M 17) are knotty and straight; #14 is superimposed on the large attached fragment #16 and does not appear to be emerging from any structure in particular. It is 8740 AU long and 1433 AU wide. It protrudes about 30° to the south of the direction to the ionizing stars. Fragment #6 in M 17 protrudes away from the cusp-like tip of a peculiar fragment (which we also labeled #6; Fig.15) and directly toward one of the ionizing stars. It is 1490 AU long and 390 AU wide. The other two jets are in NGC 2467, projecting from two attached cusps (#41 and #42) which in turn protrude from the large attached fragment #40. Both of these jets are fuzzier and smoother (rather than knotty) than the first two, and they appear to bend. Jet #42 has two ends, like the forked tongue of a snake. The double jet originates from a bright “knot” embedded in the bright limb of the cusp. It is possible that only the upper tip is the true jet, while the lower one is a chance superposition with a bright part of the region. The upper part measures 3275 AU from base to tip and has a width of 410 AU. It protrudes in a direction about 45° west of the direction to the ionizing star. The lower part is similar in length although it bends away from the ionizing source. The second fuzzy jet, #41, is peculiar in that it originates from the base, rather than the cusp of fragment #41. It measures 5730 x 1430 AU and protrudes at about 45° east of the direction to the ionizing star. All four jets are brighter in emission line luminosity (F658N) than in continuum light

(F550W).

A couple of dozen mono- and bi-polar micro-jets are found protruding from the Orion Nebula proplyds. These are smaller and less energetic than Herbig-Haro (HH) jets, which are usually found only in neutral regions. The characteristic length of the micro-jets is between 500 and 1000 AU, while their widths range between 20 and 200 AU (Bally et al. 2000). Some of them are low ionization and are found within the ionization front of the proplyd, while others extend beyond the cusp and have higher ionization levels. Most of these micro-jets are mono-polar (for a discussion of this characteristic we refer the reader to section 5.4 of Henney et al. (2002)). Most of the jets visible in the Orion nebula are micro-jets, but there are also some larger HH objects. These are seen as a series of aligned bow shocks which can extend 15 000 AU.

Our jet #14 in Pismis 24 appears intermediate between a micro-jet and a HH object. Its knotty structure could be interpreted as a series of bow shocks. Jet #6 in M 17 has a size comparable to the Orion Nebula micro-jets. The two jets in NGC 2467 have sizes that classify them as large micro-jets. However, several of their properties, such as their smooth and fuzzy appearance, do not conform with the canonical jet characteristics.

5. Summary

Here we present a summary of our findings.

- The interface between ionized gas and neutral molecular cloud in H II regions can be smooth and devoid

of fragments or sculpted and rich in fragments. This points to the fact that even the small cusps, quite similar to the proplyd cusps in the Orion Nebula, are actually fragments of molecular cloud that have recently broken off and are being photo-evaporated.

- Four bright (micro-) jet candidates might point to on-going star formation. However, none of them appear to originate from a star. Unless the absence of the star can be explained by extinction, this characteristic makes their nature suspicious. Central star aside, two of the jet candidates have all the characteristics of micro-jets, while the other two appear smoother and fuzzier than typical micro-jets observed in the Orion Nebula.
- In most of the regions studied, there is a substantial number of very small fragments. This is not consistent with the fact that the smallest fragments should be photo-evaporated the fastest and points to an active fragment production process. Fragment size distributions, such as the ones in Fig. 19, can provide constraints to theories of how molecular cloud fragments are produced.
- Tear-shaped cusps and circular silhouettes can have similar sizes (where chords are compared to diameters). We therefore suspect that these molecular cloud fragments belong to the same class, where the former is fully exposed to the ionizing radiation field, while the latter is shielded

from it. This is, however, a ballpark estimate argument and only a more accurate model could properly address this point.

- From the analysis of the optical depth properties of the circular silhouettes of Reipurth et al. (2003), we determined that the circular silhouettes in IC 2944 and possibly those in M 16 cannot be self-gravitating and collapsing to make stars. Using their assumptions about the optical depth of the fragments, we calculate Jeans lengths which are much larger than the fragment themselves, therefore pointing to their transient nature. We argue, however, that the *assumption* might actually be flawed and that the fragments might actually be rather centrally concentrated and possibly star-forming. Only in this way, would we explain the circular shapes of the silhouette fragments.
- Only one silhouette (in M 17) out of *all* the features found in the eight regions might have a central star. If this feature is indeed a proplyd (some reservations exist), it joins a small number of *bona fide* proplyds found outside the Orion Nebula. Since several of the observed regions are close enough to enable us to resolve the size of the largest proplyds found in the Orion Nebula, one might wonder why so few proplyds are found. Recent work by Smith et al. (2005) might provide an explanation. According to them, proplyds are observed only when they are close to

bright illuminating sources. However this proximity tends to evaporate them on short time scales. As a result we only see the proplyds when low mass stars have formed near massive stars *and* we observe them at the very beginning of their lives (within the first 500 000 years). The cusps we find near the cavity walls, might have been recently exposed by the advancement of the ionization front. Their placental material is externally ionized and evaporated giving them a limb-brightened appearance. Eventually, the nascent star in their middle will be completely stripped (surrounded by a disk or not) but will not shine as a proplyd because it is not sufficiently close to the ionizing source (for further elaborations on this point, the reader is referred to Johnstone et al. 1998).

We are thankful to David Zurek for spotting fragment #12 in M 17, a possible *bona fide* circumstellar disk around a young star and for carrying out the early data reduction on the M 17 ERO observations that helped us write the proposal that led to the current dataset. We acknowledge useful discussion with Hector Harce and Mordecai-Mark Mac Low. We thank Katie Ray and Geoff Clayton for reading and commenting on the manuscript and the Referee, Will Henney, for comments that improved the paper. RHR acknowledges support from the NASA Long-Term Space Astrophysics (LTSA) program. This work was supported by an HST grant associated with proposal GO-9857. This research has

made use of the SIMBAD database, operated at CDS, Strasbourg, France

REFERENCES

- Abt, H. A. & Corbally, C. J. 2000, ApJ, 541, 841
- Allen, D. A. 1986, MNRAS, 219, 35P
- Ardeberg, A. & Maurice, E. 1980, A&AS, 39, 325
- Bally, J., Licht, D., Smith, N., & Walawender, J. 2005, AJ, 129, 355
- Bally, J., O'Dell, C. R., & McCaughrean, M. J. 2000, AJ, 119, 2919
- Bally, J., Yu, K. C., Rayner, J., & Zinnecker, H. 1998, AJ, 116, 1868
- Belikov, A. N., Kharchenko, N. V., Piskunov, A. E., & Schilbach, E. 1999, A&AS, 134, 525
- . 2000, A&A, 358, 886
- Bica, E., Dutra, C. M., & Barbuy, B. 2003, A&A, 397, 177
- Bok, B. J. & Reilly, E. F. 1947, ApJ, 105, 255
- Brandner, W., Grebel, E. K., Chu, Y.-H., Dottori, H., Brandl, B., Richling, S., Yorke, H. W., Points, S. D., & Zinnecker, H. 2000, AJ, 119, 292
- Carraro, G., Patat, F., & Baumgardt, H. 2001, A&A, 371, 107
- Clemens, D. P., Yun, J. L., & Heyer, M. H. 1991, ApJS, 75, 877

- Cruz-Gonzalez, C., Recillas-Cruz, E., Costero, R., Peimbert, M., & Torres-Peimbeert, S. 1974, *Revista Mexicana de Astronomia y Astrofisica*, 1, 211
- Dutra, C. M., Bica, E., Soares, J., & Barbuy, B. 2003, *A&A*, 400, 533
- Feinstein, A. & Vazquez, R. A. 1989, *A&AS*, 77, 321
- Guetter, H. H. & Turner, D. G. 1997, *AJ*, 113, 2116
- Hanson, M. M., Howarth, I. D., & Conti, P. S. 1997, *ApJ*, 489, 698
- Henney, W. J. & O'Dell, C. R. 1999, *AJ*, 118, 2350
- Henney, W. J., O'Dell, C. R., Meaburn, J., Garrington, S. T., & Lopez, J. A. 2002, *ApJ*, 566, 315
- Hester, J. J., Scowen, P. A., Sankrit, R., Lauer, T. R., Ajhar, E. A., Baum, W. A., Code, A., Currie, D. G., Danielson, G. E., Ewald, S. P., Faber, S. M., Grillmair, C. J., Groth, E. J., Holtzman, J. A., Hunter, D. A., Kristian, J., Light, R. M., Lynds, C. R., Monet, D. G., O'Neil, E. J., Shaya, E. J., Seidemann, K. P., & Westphal, J. A. 1996, *AJ*, 111, 2349
- Jeans, J. H. 1902, *Philos. Trans. R. Soc. London A*, 199, 1
- Johnstone, D., Hollenbach, D., & Bally, J. 1998, *ApJ*, 499, 758
- Joye, W. A. & Mandel, E. 2003, in *ASP Conf. Ser. 295: Astronomical Data Analysis Software and Systems XII*, 489–+
- Lodén, L. O. 1966, *Arkiv for Astronomi*, 4, 65
- Maíz-Apellániz, J., Walborn, N. R., Galué, H. Á., & Wei, L. H. 2004, *ApJS*, 151, 103
- Massey, P., DeGioia-Eastwood, K., & Waterhouse, E. 2001, *AJ*, 121, 1050
- McCaughrean, M. J. & O'Dell, C. R. 1996, *AJ*, 111, 1977
- O'Dell, C. R. 2001, *ARA&A*, 39, 99
- O'Dell, C. R., Wen, Z., & Hu, X. 1993, *ApJ*, 410, 696
- Paladini, R., Burigana, C., Davies, R. D., Maino, D., Bersanelli, M., Cappellini, B., Platania, P., & Smoot, G. 2003, *A&A*, 397, 213
- Pellerin, A., Fullerton, A. W., Robert, C., Howk, J. C., Hutchings, J. B., Walborn, N. R., Bianchi, L., Crowther, P. A., & Sonneborn, G. 2002, *ApJS*, 143, 159
- Reid, I. N., Brewer, C., Brucato, R. J., McKinley, W. R., Maury, A., Mendenhall, D., Mould, J. R., Mueller, J., Neugebauer, G., Phinney, J., Sargent, W. L. W., Schombert, J., & Thicksten, R. 1991, *PASP*, 103, 661
- Reipurth, B., Corporon, P., Olberg, M., & Tenorio-Tagle, G. 1997, *A&A*, 327, 1185
- Reipurth, B., Raga, A., & Heathcote, S. 2003, *AJ*, 126, 1925
- Schild, R. E., Garrison, R. F., & Hiltner, W. A. 1983, *ApJS*, 51, 321
- Smith, N., Bally, J., & Morse, J. A. 2003, *ApJ*, 587, L105

- Smith, N., Bally, J., Shuping, R. Y., Morris, M., & Kassis, M. 2005, *AJ*, 130, 1763
- Stapelfeldt, K., Sahai, R., Werner, M., & Trauger, J. 1997, in *ASP Conf. Ser. 119: Planets Beyond the Solar System and the Next Generation of Space Missions*, 131–+
- Stecklum, B., Henning, T., Feldt, M., Hayward, T. L., Hoare, M. G., Hofner, P., & Richter, S. 1998, *AJ*, 115, 767
- Sung, H., Chun, M.-Y., & Bessell, M. S. 2000, *AJ*, 120, 333
- Thackeray, A. D. 1950, *MNRAS*, 110, 524
- Tody, D. 1986, in *Instrumentation in astronomy VI; Proceedings of the Meeting, Tucson, AZ, Mar. 4-8, 1986. Part 2 (A87-36376 15-35)*. Bellingham, WA, Society of Photo-Optical Instrumentation Engineers, 1986, p. 733., 733–+
- Tody, D. 1993, in *ASP Conf. Ser. 52: Astronomical Data Analysis Software and Systems II*, 173–+
- van den Ancker, M. E., The, P. S., Feinstein, A., Vazquez, R. A., de Winter, D., & Perez, M. R. 1997, *A&AS*, 123, 63
- Vannier, L., Lemaire, J. L., Field, D., Pineau des Forêts, G., Pijpers, F. P., & Rouan, D. 2001, *A&A*, 366, 651
- Vázquez-Semadeni, E., Kim, J., Shadmehri, M., & Ballesteros-Paredes, J. 2005, *ApJ*, 618, 344
- Walborn, N. R. 1972, *AJ*, 77, 312
- . 1982, *AJ*, 87, 1300
- . 1987, *AJ*, 93, 868
- Warren, W. H. & Hesser, J. E. 1977, *ApJS*, 34, 115
- Yusef-Zadeh, F., Biretta, J., & Geballe, T. R. 2005, *AJ*, 130, 1171

This 2-column preprint was prepared with the AAS L^AT_EX macros v5.2.

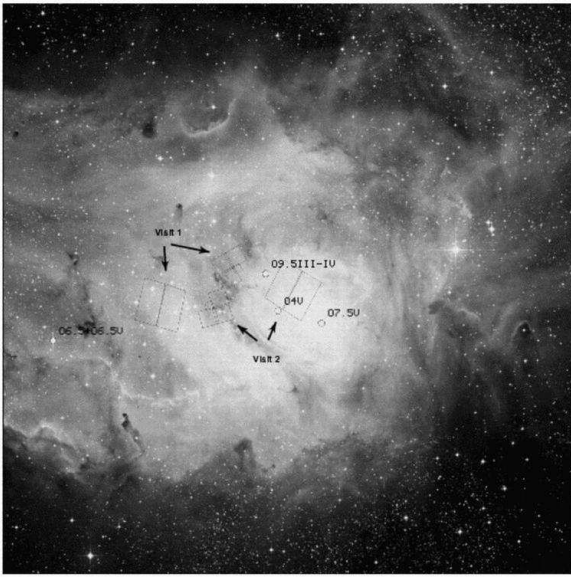


Fig. 1.— A 45x45 arcmin² DSS/POSSII (red filter) image of NGC 6530 (Visits 1 and 2), with an overlay of the ACS and WFPC2 apertures used. North is toward the top, east toward the left. The O stars are marked (see Table 3).

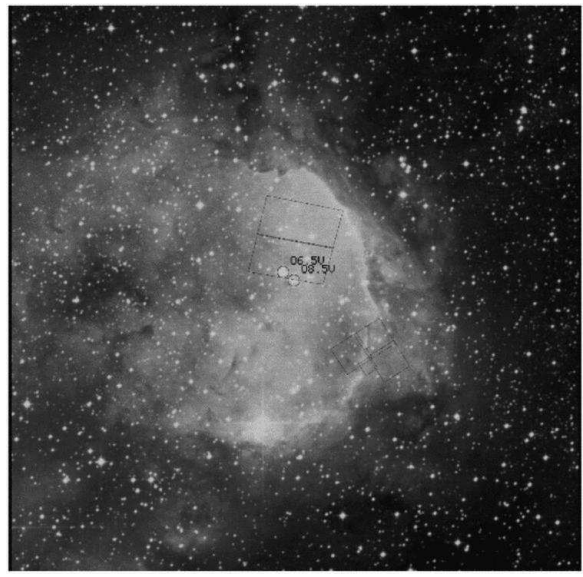


Fig. 2.— A 25x25 arcmin² DSS/POSSII (red filter) image of NGC 3324, with an overlay of the ACS and WFPC2 apertures used. North is toward the top, east toward the left. The O stars are marked (see Table 3).

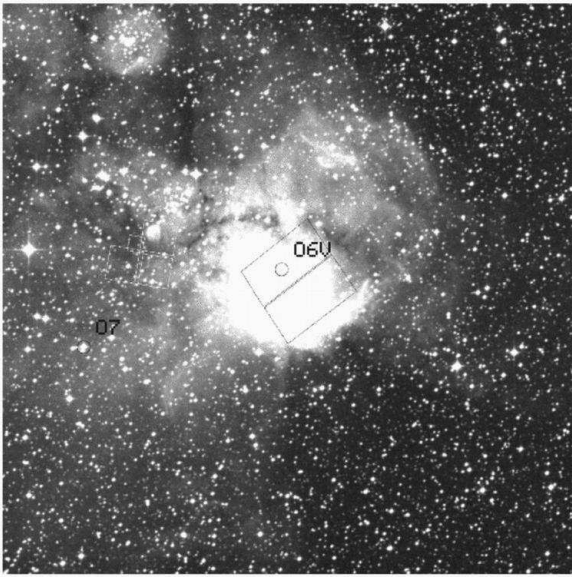


Fig. 3.— A 25x25 arcmin² DSS/POSSII (red filter) image of NGC 2467 with an overlay of the ACS and WFPC2 apertures used. North is toward the top, east toward the left. The O stars are marked (see Table 3).

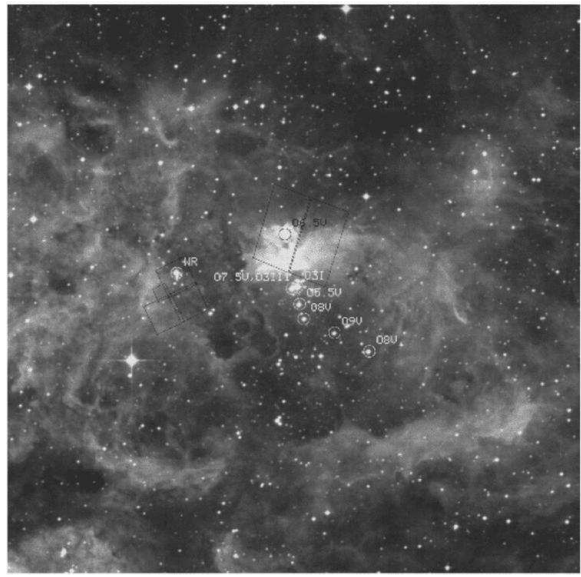


Fig. 4.— A 25x25 arcmin² DSS/POSSII (red filter) image of Pismis 24 with an overlay of the ACS and WFPC2 apertures used. North is toward the top, east toward the left. The O stars and one Wolf-Rayet star are marked (see Table 3).



Fig. 5.— A 25×25 arcmin² DSS/POSSII (red filter) image of IC 1590 with an overlay of the ACS and WFPC2 apertures used. North is toward the top, east toward the left. The O stars are marked (see Table 3).



Fig. 6.— A 25×25 arcmin² DSS/POSSII (red filter) image of IC 2944 with an overlay of the WFPC2 apertures used. North is toward the top, east toward the left. The O stars are marked (see Table 3).



Fig. 7.— A 25×25 arcmin² DSS/POSSII (red filter) image of M 16 with an overlay of the WFPC2 apertures used by programs GO9091 and GO7381. North is toward the top, east toward the left. The O stars are marked (see Table 3).

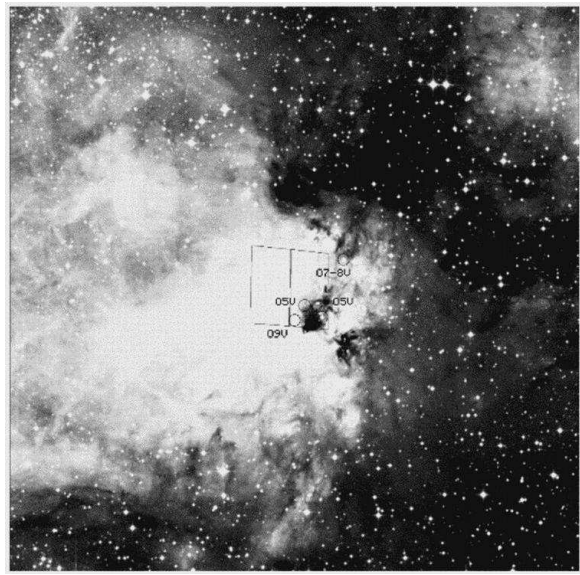


Fig. 8.— A 25×25 arcmin² DSS/POSSII (red filter) image of M 17 with an overlay of the ACS aperture used by program GO8992. North is toward the top, east toward the left. The O stars are marked (see Table 3).

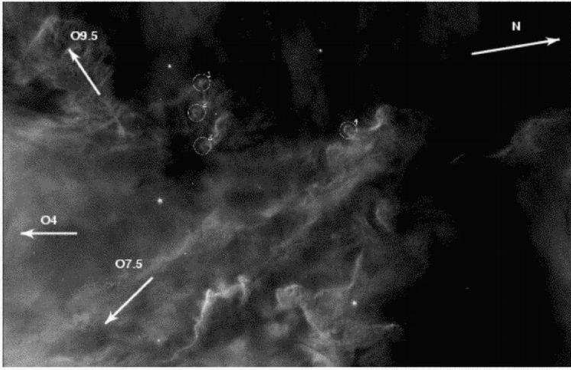


Fig. 9.— A 100×65 arcsec² part of the ACS/H α image of NGC 6530 (Visit 2; pixel ranges $x=2055-4075$, $y=530-1830$ of the ACS chip). North is indicated, east is left of north. The marked feature numbers refer to the IDs in Table 4. Approximate directions (arrows) to the main ionizing stars (labeled) are shown. For the exact location of the stars refer to Fig. 1.

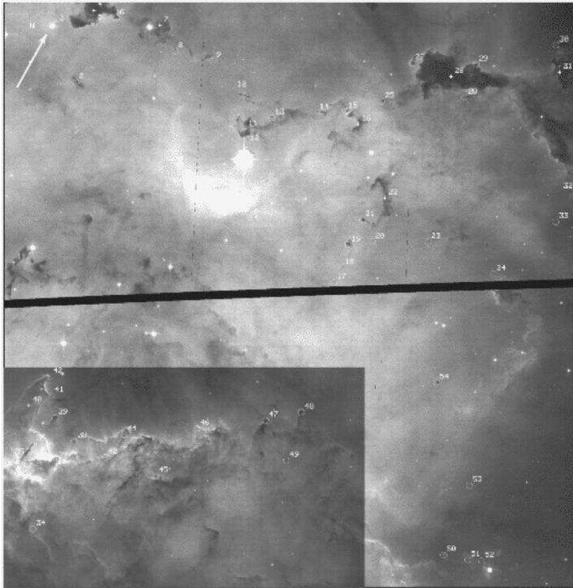


Fig. 10.— The ACS/H α image of NGC 2467. North is indicated, east is left of north. The marked feature numbers refer to the IDs in Table 4. The main ionizing star is labeled. The lower portion of the image is displayed with a larger greyscale stretch to provide details in the brightest regions.

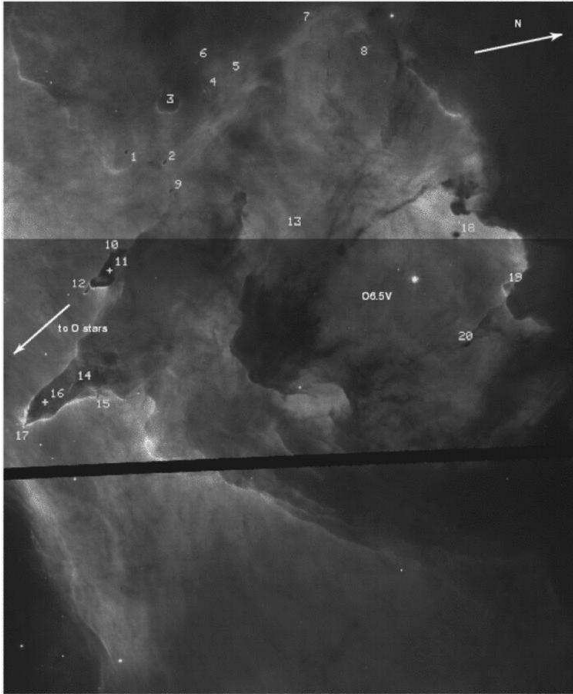


Fig. 11.— A 110×75 arcsec² portion of the ACS/H α image of Pismis 24 (pixel ranges $x=229-2629$, $y=1135-4031$ of the ACS chip). North is indicated, east is left of north. The marked feature numbers refer to the IDs in Table 4. The approximate direction (arrow) to the main ionizing stars is shown, as is one O star within the FOV. For the exact location of the stars refer to Fig. 4. The upper and lower parts of the image are displayed with a different gray-scale stretch.

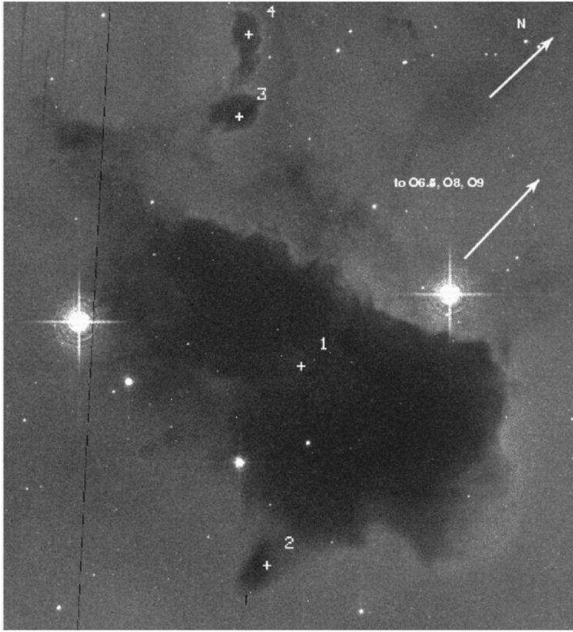


Fig. 12.— A 50×55 arcsec² portion of the ACS/H α image of IC 1590 (pixel ranges $x=1390-2390$, $y=2760-3860$ of the ACS chip). North is indicated, east is left of north. The marked feature numbers refer to the IDs in Table 4. Approximate directions (arrow) to the main ionizing stars (labeled) are shown. For the exact location of the stars refer to Fig. 5. O stars within the FOV are labeled.

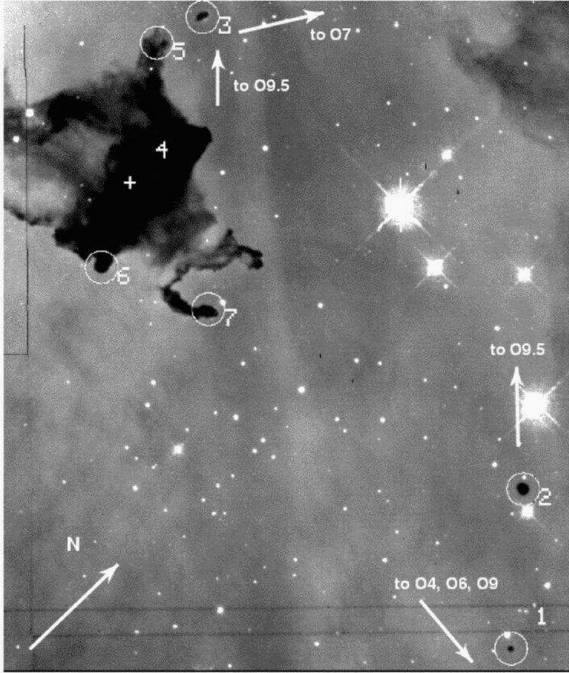


Fig. 13.— A 35×40 arcsec² portion of the WFPC2/H α image of M 16 from program GO7381 (cropped to display the pixel ranges $x=760-1460$, $y=710-1530$). North is indicated, east is left of north. The marked feature numbers refer to the IDs in Table 4. Approximate directions (arrows) to the main ionizing stars (labeled) are shown. For the exact location of the stars refer to Fig. 7.

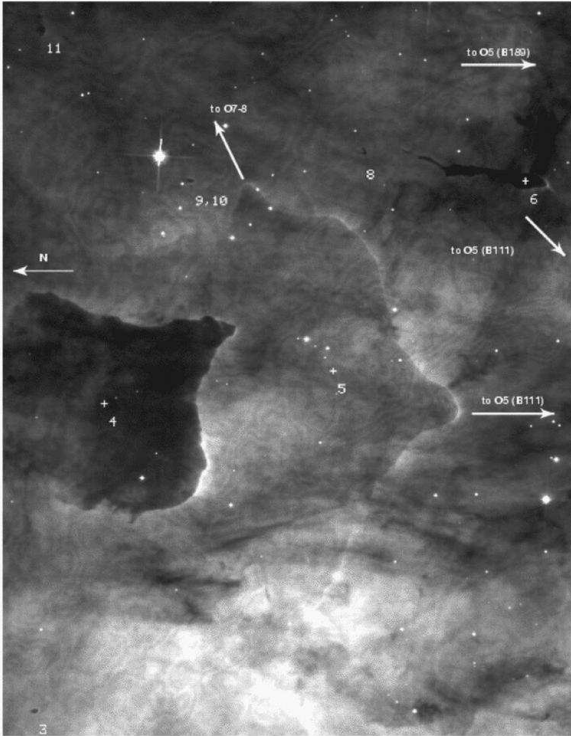


Fig. 14.— An 80×60 arcsec² portion of the ACS image of M 17 (image j8cw07041_drz.fits, rotated by 90 degrees, and cropped to display the pixel ranges $x=444-1716$, $y=2558-4206$). North is indicated, east is left of north. The marked feature numbers refer to the IDs in Table 4. Approximate directions (arrows) to the main ionizing stars (labeled) are shown. For the exact location of the stars refer to Fig. 8.

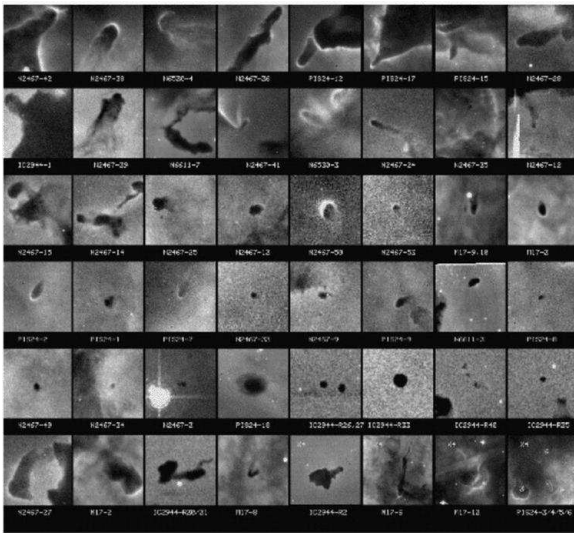


Fig. 15.— Subset of the features identified in the H II regions. Each stamp is 5 arcsec on a side, except for the last four “stamps” which are 20 arcsec (marked x4). Stamp labels refer to the region within which the features are found and the IDs from Table 4. For an explanation of the layout see Sec. 3.

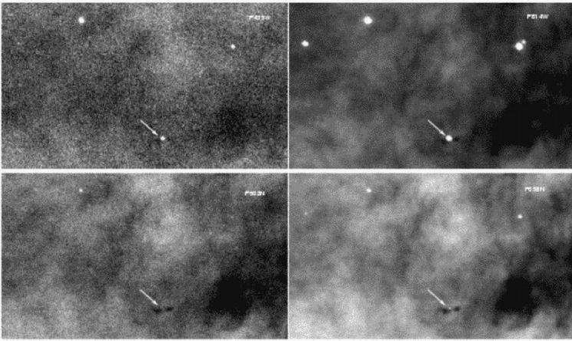


Fig. 16.— A 16×11 arcsec² portion of the ACS image of M 17 in the immediate area of M 17-12 (Table 4) which is located at pixel position (2022,3844), imaged through four different filters (labeled). North is toward the right, east is up. The arrows point to the putative star with disk.

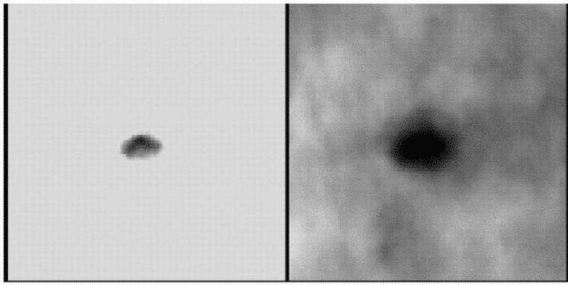


Fig. 17.— A 5×5 arcsec² portion of the ACS/H α image of M 17, centered around feature 7. Two greyscale levels are used to show both the boomerang shape of the darkest absorption (left panel) and the rounded shape of the overall feature (right panel).

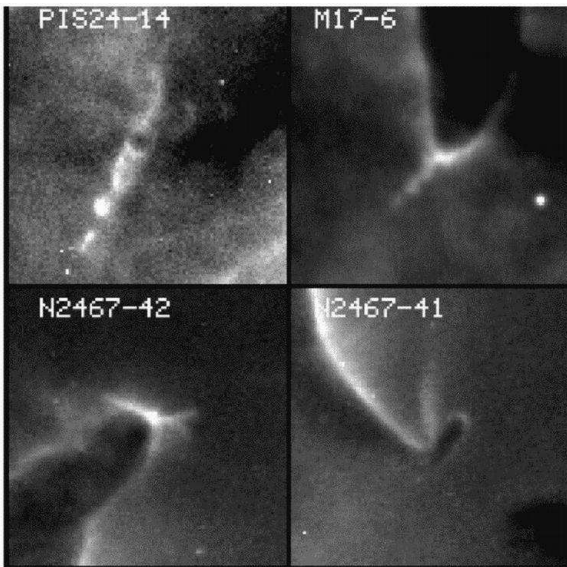


Fig. 18.— 5×5 arcsec² images of the four jets observed in the H II regions. North is oriented as in Figs.11 (Pismis 24), 14 (M 17), and 10 (NGC 2467). Labels refer to the regions as well as the ID numbers from Table 4. The jets are discussed in Section 4.4.

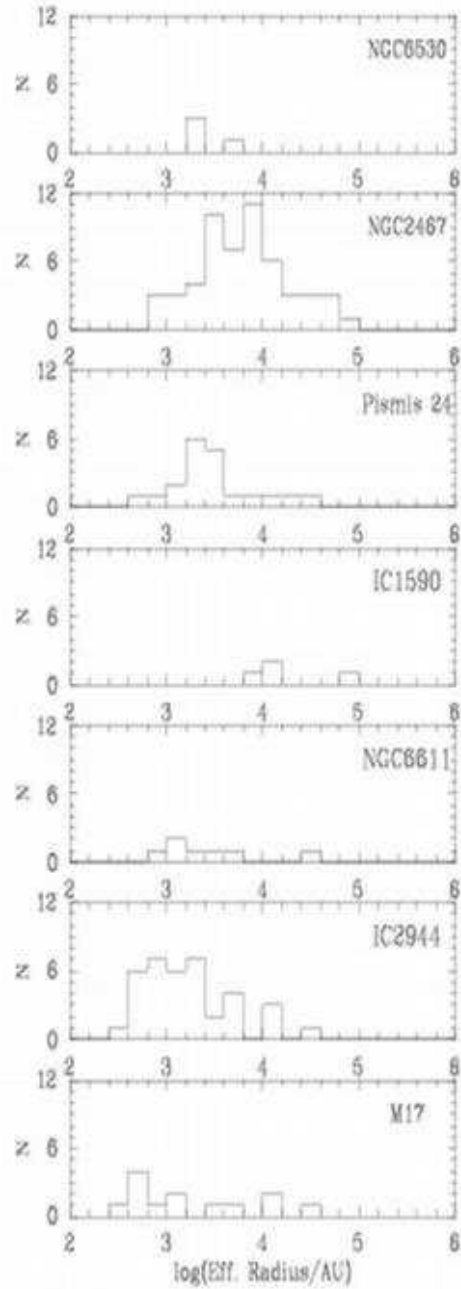


Fig. 19.— A histogram of the $\log(\text{Effective Radius})$ of fragments found in each region. Those regions with insufficient number of fragments to determine the distribution are displayed to compare the sizes of the fragment with those of the other regions.

TABLE 1
OBSERVING LOG.

Object	RA & Dec (J2000)	PA (deg)	Instrument	Filter	UT Date	Exposure time (sec)
Complete image set from program GO 9857						
NGC 6530-V1	18 04 54.87 -24 17 17.3	299.9	WFPC2	F656N	2004-04-04	525
NGC 6530-V1	18 04 31.50 -24 21 15.7	255.0	ACS/WFC	F658N	2004-04-04	780
NGC 6530-V1	18 04 31.50 -24 21 15.7	255.0	ACS/WFC	F660N	2004-04-04	800
NGC 6530-V1	18 04 31.50 -24 21 15.7	255.0	ACS/WFC	F550N	2004-04-04	400
NGC 6530-V2	18 04 13.21 -24 21 40.0	104.8	WFPC2	F656N	2003-07-07	525
NGC 6530-V2	18 03 49.20 -24 19 53.0	60.0	ACS/WFC	F658N	2003-07-07	780
NGC 6530-V2	18 03 49.20 -24 19 53.0	60.0	ACS/WFC	F660N	2003-07-07	800
NGC 6530-V2	18 03 49.20 -24 19 53.0	60.0	ACS/WFC	F550N	2003-07-07	400
NGC 3324	10 36 51.40 -58 40 43.9	214.6	WFPC2	F656N	2004-08-19	851
NGC 3324	10 37 18.50 -58 36 11.0	169.8	ACS/WFC	F658N	2004-08-19	1300
NGC 3324	10 37 18.50 -58 36 11.0	169.8	ACS/WFC	F660N	2004-08-19	1960
NGC 3324	10 37 18.50 -58 36 11.0	169.8	ACS/WFC	F550N	2004-08-19	654
NGC 2467	07 52 44.35 -26 25 12.5	79.8	WFPC2	F656N	2004-02-18	410
NGC 2467	07 52 18.20 -26 26 06.0	35.0	ACS/WFC	F658N	2004-02-18	750
NGC 2467	07 52 18.20 -26 26 06.0	35.0	ACS/WFC	F660N	2004-02-18	897
NGC 2467	07 52 18.20 -26 26 06.0	35.0	ACS/WFC	F550N	2004-02-18	340
Pismis 24	17 25 09.30 -34 12 15.7	114.4	WFPC2	F656N	2003-07-08	505
Pismis 24	17 24 43.60 -34 09 40.5	69.6	ACS/WFC	F658N	2003-07-08	685
Pismis 24	17 24 43.60 -34 09 40.5	69.6	ACS/WFC	F660N	2003-07-08	960
Pismis 24	17 24 43.60 -34 09 40.5	69.6	ACS/WFC	F550N	2003-07-08	350
IC 1590	00 53 30.64 56 37 30.1	76.0	WFPC2	F656N	2004-03-02	605
IC 1590	00 52 49.00 56 36 12.7	31.1	ACS/WFC	F658N	2004-03-02	678
IC 1590	00 52 49.00 56 36 12.7	31.1	ACS/WFC	F660N	2004-03-02	1017
IC 1590	00 52 49.00 56 36 12.7	31.1	ACS/WFC	F550M	2004-03-02	450
Selected archival images used						
IC 2944	11 38 22.25 -63 20 37.2	14.8	WFPC2	F656N	1999-02-07	452 ^a
M 16	18 18 42.13 -13 47 58.6	143.8	WFPC2	F656N	2002-08-08	2600 ^b
M 17	18 20 34.91 -16 09 27.54	267.1	ACS/WFC	F658N	2002-04-01	760
M 17	18 20 34.91 -16 09 27.54	267.1	ACS/WFC	F502N	2002-04-02	760
M 17	18 20 34.91 -16 09 27.54	267.1	ACS/WFC	F435W	2002-04-01	710
M 17	18 20 34.91 -16 09 27.54	267.1	ACS/WFC	F814W	2002-04-01	720

^aFrom averaging the eight available H α images.

^bFrom averaging the four available H α images.

TABLE 2
CLUSTER/H II REGION PARAMETERS.

Name	RA & Dec ^a (J2000)	Distance ±error (kpc)	Age [age spread] (Myr)	Diameter HII (pc)	O Star ^b content	Earliest spectral type	FOV (pc)	3-pixels ^c (AU)
NGC 6530 ^d	18 04 48 -24 20	1.8±0.1	1.5[4.0]	18	3E/2L	O4 V	1.8	270
NGC 3324 ^e	10 37 18 -58 38	3.0±0.1	<2-3	12	1E/1L	O6.5 V	3.0	450
NGC 2467	07 52 19 -26 26 30	4.1 ^f	12:: ^g	8	1E/1L	O6 V	4.1	610
Pismis 24 ^h	17 25 24 -34 26	2.5	0.7[2.3]	50/2.5	4E/4L	O3 I,III	2.5	370
IC 1590 ^j	00 53 03 +56 35	2.94±0.15	3.5±0.2	21	1E/2L	O6.5 V	2.9	440
IC 2944 ^k	11 38 20 -63 22 22	1.8 ^l	7	28	4E/5L	O6 V	0.60	230
M 16	18 18 48 -13 47	2.14±0.10 ^m	6[6] ⁿ	18	3E/6L	O4 V	0.87	330
M 17 ^o	18 20 26 -16 10 36	1.3	1	37	2E/2L	O5	1.3	190

^aThese are the ICRS coordinates from the SIMBAD database.

^b“E” stands for Early (O3-O6), “L” stands for late (O7-O9). The number indicates how many early or late O stars are present in the region.

^cSize of 3-pixels in AU. This is the minimum detection size of a fragment.

^dSung et al. 2000.

^eCarraro et al. 2001.

^fFeinstein & Vasquez 1989.

^gLodén 1966; very uncertain.

^hMassey et al. 2001.

^jGuetter & Turner 1997.

^kWalborn 1987.

^lArdeberg & Maurice 1980.

^mBelikov et al. 1999.

ⁿBelikov et al. 2000.

^oHanson et al. 1997.

TABLE 3
O STARS IN THE OBSERVED REGIONS.

Name (Alias)	RA & Dec (J2000)	V Magnitudes (mag)	Spectral Type ^a	Reference
NGC 6530				
HD164740 (Her 36)	18 03 40.2 -24 22 43	9.1	O7.5 V	Walborn 1982
HD164794 (9 Sgr)	18 03 52.4 -24 21 38	5.96	O4 V((f))	Walborn 1972; Schild et al. 1983
HD164816	18 03 56.9 -24 18 45	7.09	O9.5 III-IVn	Maíz-Apellániz et al. 2004
HD166052	18 05 10.5 -24 23 54	6.9	O6.5+O6.5 V	van den Ancker et al. 1997
NGC 3324				
HD092206AB	10 37 22.3 -58 37 23	7.82	O6.5 V(n)	Maíz-Apellániz et al. 2004
HD092206C	10 37 18.6 -58 37 42	-	O8.5 Vp	Maíz-Apellániz et al. 2004
NGC 2467				
HD64315	07 52 20.3 -26 25 46	9.19	O6 Vn	Walborn 1982
CD-26 5129	07 52 55.4 -26 28 42	9.39	O7	Feinstein & Vazquez 1989
Pismis 24				
Cl Pismis 24 15	17 24 28.7 -34 14 50	12.32	O8 V	Massey et al. 2001
Cl Pismis 24 10	17 24 35.9 -34 13 59	13.02	O9 V	Massey et al. 2001
Cl Pismis 24 3	17 24 42.2 -34 13 21	12.75	O8 V	Massey et al. 2001
HD319718	17 24 42.9 -34 11 48	10.43	O3 If*	Massey et al. 2001
Cl Pismis 24 2	17 24 43.2 -34 12 43	11.95	O5.5 V((f))	Massey et al. 2001
Cl Pismis 24 16 (N58)	17 24 44.3 -34 12 00	13.02	O7.5 V	Massey et al. 2001
Cl Pismis 24 17 (N57)	17 24 44.7 -34 12 02	11.84	O3 III(f*)	Massey et al. 2001
Cl Pismis 24 13 (N36)	17 24 45.7 -34 09 39	12.73	O6.5 V((f))	Massey et al. 2001
HD157504 (WR 93)	17 25 08.9 -34 11 12	11.46	WC7+abs?	Massey et al. 2001
IC 1590 ^b				
HD5005AB	00 52 49.2 +56 37 39	8.34	O6.5 V((f))	Guetter & Turner 1997
HD5005C	00 52 49.4 +56 37 39	9.19	O8 Vn	Guetter & Turner 1997
HD5005D	00 52 49.6 +56 37 36	9.78	O9 Vn	Guetter & Turner 1997
IC 2944				
HD101131	11 37 48.4 -63 19 23	7.14	O6 V((f))	Maíz-Apellániz et al. 2004
HD308813	11 37 58.4 -63 18 59	9.28	O9.5 V	Pellerin et al. 2002
HD101190	11 38 09.9 -63 11 48	7.31	O6 V((f))	Maíz-Apellániz et al. 2004
HD101191	11 38 12.2 -63 23 26	8.49	O8 V((n))	Maíz-Apellániz et al. 2004
HD101205	11 38 20.4 -63 22 21	6.46	O7 IIIIn((f))	Maíz-Apellániz et al. 2004
HD101223	11 38 22.8 -63 12 02	8.69	O8 V((f))	Maíz-Apellániz et al. 2004
HD101298	11 39 03.3 -63 25 47	8.07	O6 V((f))	Maíz-Apellániz et al. 2004
HD101413	11 39 45.8 -63 28 40	8.35	O8 V	Maíz-Apellániz et al. 2004
HD101436	11 39 49.9 -63 28 43	7.59	O6.5 V	Maíz-Apellániz et al. 2004
M 16				
BD-13 4921	18 18 29.9 -13 49 57	9.85	O9 V	Cruz-Gonzalez et al. 1974
NGC 6611 166	18 18 32.2 -13 48 48	10.35	O9 V	Cruz-Gonzalez et al. 1974
BD-13 4923	18 18 32.7 -13 45 12	10.08	O6	Cruz-Gonzalez et al. 1974
HD168075	18 18 36.1 -13 47 36	8.75	O6 V((f))	Maíz-Apellániz et al. 2004
HD168076	18 18 36.4 -13 48 02	8.20	O4 V((f))	Maíz-Apellániz et al. 2004
BD-13 4927	18 18 40.1 -13 45 18	9.55	O7 Ib(f)	Maíz-Apellániz et al. 2004
BD-13 4929	18 18 45.9 -13 46 31	9.86	O9.5 V	Cruz-Gonzalez et al. 1974
BD-13 4930	18 18 52.7 -13 49 42	9.44	O9.5 V	Cruz-Gonzalez et al. 1974
HD168137	18 18 56.2 -13 48 31	8.95	O8 V	Cruz-Gonzalez et al. 1974
M 17				
Cl* NGC 6618 B 260	18 20 26.0 -16 08 32	14.20	O7-8 V	Hanson et al. 1997

TABLE 3—*Continued*

Name (Alias)	RA & Dec (J2000)	V Magnitudes (mag)	Spectral Type ^a	Reference
Cl* NGC 6618 B 189	18 20 29.8 -16 10 44	14.13	O5 V	Hanson et al. 1997
Cl* NGC 6618 B 111	18 20 34.5 -16 10 12	11.29	O5 V	Hanson et al. 1997
Cl* NGC 6618 B 98	18 20 35.4 -16 10 48	10.1	O9 V	Hanson et al. 1997

^aThe spectral type notation, originally from Walborn (1972), is also explained in the listed references.

^bThere is a great deal of confusion about how many stars reside in this tight cluster. For instance, one would believe that Tr 13, cited by Abt & Corbally (2000) is an additional star but this star, also called ADS719, appears cross-referenced to HD5005 in the SIMBAD database. Therefore we only list the stars from Guetter & Turner (1997), cautioning that this might provide only a lower limit to the stellar content and number of hard photons in this region.

TABLE 4
DISCRETE FEATURES DETECTED IN THE OBSERVED REGIONS.

ID	Class	Shape	Edges	Location	Short & Long ^a dimensions (AU)	(X,Y) ^b position (pix)
NGC 6530						
1	cusp	-	LB	attached ridge	1530 2700	2808 1336
2	cusp	-	LB	attached ridge	990 3600	2761 1313
3	cusp	-	LB	attached ridge	900 3330	2764 731
4	cusp	rounded	LB	attached ridge	2700 9001	2901 1038
NGC 2467						
1	fragment	complex	mix	isolated	6561 38954	333 2349
2	sil.	irregular	fuzzy	near frag. 4	2050 21732	741 3536
3	sil.	nodule	sharp	near frag. 4	1025	613 3918
4	fragment	complex	mix	near frag. 7	33828 59045	864 4006
5	cusps	rounded	LB	attached frag. 4	1763 2870	865 3923
6	cusp	rounded	LB	attached frag. 4	4510 8611	1009 3956
7	fragment	complex	mix	near frag. 4	20502 45104	1300 3910
8	sil.	-	fuzzy	attached frag. 7	2952 5330	1390 3743
9	cusp	rounded	LB	near frag. 7	820	1646 3679
10	fragment	complex	mix	near frag. 11	11071 29113	1847 3445
11	fragment	complex	mix	near frag. 16	20502 94309	1857 3225
12	cusp	rounded	LB	attached frag.11	1435 9841	1866 3128
13	cusp	rounded	LB	near frag. 11	4100	2032 3301
14	fragment	complex	mix	near frag. 16	8201 22142	2325 3336
15	cusp	rounded	LB	attached frag.16	4100 7381	2515 3344
16	fragment	complex	mix	near frag. 26	6151 61506	2603 3259
17	sil.	rounded	fuzzy	isolated	3403	2440 2219
18	sil.	rounded	sharp	isolated	2132	2493 2314
19	sil.	triangular	sharp	near frag. 22	6561	2535 2465
20	sil.	nodule	sharp	near frag. 22	1804	2693 2486
21	sil.	complex	sharp	attached frag.22	4510 32803	2627 2631
22	fragment	complex	mix	isolated	10251 73807	2779 2773
23	cusp	complex	LB	isolated	5741	3061 2483
24	cusp	-	LB	attached ridge	2132 8201	3491 2275
25	cusp	complex	LB	near frag. 26	4920	2757 3409
26	fragment	complex	mix	attached ridge	40184 102509	3215 3573
27	fragment	complex	LB	attached frag.26	4920 17222	2956 3660
28	cusp	-	LB	attached frag.26	4510 13531	3303 3435
29	cusp	hooked	LB	attached frag.26	2050 5741	3375 3652
30	cusp	rounded	LB	attached ?	5741 7791	3901 3774
31	fragment	complex	mix	near ridge	28703 41004	3930 3602
32	cusp	-	LB	near ridge	5330 25422	3981 2815
33	cusp	-	LB	near ridge	1845	3901 2615
34	sil.	nodule	sharp	near ridge	1148	459 596
35	cusp	-	LB	attached ridge	1230 6151	319 1064
36	cusp	-	LB	attached ridge	2870 28293	460 1154
37	cusp	-	LB	attached ridge	6971 15171	606 1041
38	cusp	-	LB	attached ridge	4510 22552	732 1173
39	cusp	multi-tip	sharp	near ridge	5741 14761	605 1328
40	fragment	complex	mix	attached ridge	26652 82007	436 1408
41	cusp	w/ jet	LB	attached ridge	1271 5741	582 1474

TABLE 4—*Continued*

ID	Class	Shape	Edges	Location	Short & Long ^a dimensions (AU)	(X,Y) ^b position (pix)
42	cuspid	-	LB	attached frag.	4920 10661	571 1599
43	cuspid	hooked	LB	attached ridge	2460 4100	933 1067
44	cuspid	-	LB	attached ridge	6151 20912	1059 1219
45	cuspid	-	LB	attached ridge	2460 4920	1268 945
46	cuspid	pointy	LB	attached ridge	16401 4100	1540 1256
47	cuspid	3-tip	LB	attached ridge	9021 29933	1992 1310
48	cuspid	2-tip	LB	attached ridge	5330 18042	2226 1364
49	sil.	circular	sharp	near ridge	1599	2128 1046
50	cuspid	-	LB	near ridge	4510	3162 424
51	cuspid	long	LB	near ridge	3690 15171	3322 393
52	cuspid	-	LB	near ridge	820 1230	3413 387
53	cuspid	-	LB	near ridge	2460	3334 881
54	cuspid	-	LB	near ridge	4100 5741	3117 1559
Pismis 24						
1	cuspid	rounded	LB	near ridge	1900	743 3395
2	cuspid	-	LB	near ridge	1500 4000	902 3349
3	cuspid	rounded/tail	LB	near ridge	12501 15001	915 3601
4	cuspid	long	LB	near ridge	2000 7751	1073 3658
5	cuspid	-	LB	near ridge	750 2250	1169 3723
6	cuspid	-	LB	near ridge	1900	1033 3777
7	cuspid	-	LB	near ridge	2125 4000	1463 3930
8	cuspid	-	LB	near ridge	499	1703 3786
9	cuspid	-	LB	near ridge	1775 3000	928 3231
10	cuspid	-	LB	attached	1800 3250	680 2981
11	fragment	complex	LB	attached ridge	12001 32503	677 2908
12	cuspid	-	LB	attached	1850 5000	576 2818
13	sil.	nodule	sharp	-	475 1900	1396 3076
14	cuspid	long/knotty	LB	attached	1450 6001	521 2432
15	cuspid	pointy	LB	attached	2500	624 2379
16	fragment	complex	LB	attached ridge	15001 67506.	408 2359
17	cuspid	-	LB	attached	1375	317 2558
18	sil.	circular/halo	sharp	near ridge	3250	2120 3049
19	cuspid	pointy	LB	attached ridge	2500 5500	2317 2843
20	sil.	cuspid-like	fuzzy	attached ridge	2500 25002	2148 2594
IC 1590						
1	fragment	complex	LB	isolated ?	55865 138192	1913 3220
2	cuspid	rounded	LB	attached frag. 1	7645 17936	1853 2872
3	fragment	rounded	LB	near frag. 1	8530	1805 3656
4	fragment	rounded	LB	near frag. 1	6760 19700	1821 3800
IC 2944 ^c						
R1	fragment	complex	sharp	isolated	30603 48604	1465 837
R2	fragment	complex	sharp	isolated	10441 18002	319 161
R3	fragment	complex	sharp	isolated	9361 27002	976 201
R11	fragment	complex	sharp	isolated	1980 15841	553 418
R11B	cuspid	hooked	LB	attached frag.11	774 1764	544 325
R14	sil.	complex	sharp	-	4320 6373	857 845
R15	sil.	complex	sharp	-	1800	963 831

TABLE 4—*Continued*

ID	Class	Shape	Edges	Location	Short & Long ^a dimensions (AU)	(X,Y) ^b position (pix)
R16	sil.	circular	sharp	-	1980	913 1384
1	sil.	rounded	sharp	attached frag. 1	1980 2880	945 1228
R17	sil.	circular	sharp	-	1368	1024 1340
R18	fragment	complex	fuzzy	attached frag. 1	3240 4500	1103 1437
R19	sil.	circular	sharp	-	1260	1190 1490
R20	sil.	rounded	fuzzy	-	2160	1370 1371
R21	sil.	circular	sharp	-	990	1499 1219
R22	sil.	complex	sharp	-	4500 5761	1438 1127
2	sil.	nodule	sharp	-	720	1384 1171
R23	sil.	long	sharp	-	900 3960	1434 891
R24	sil.	long	sharp	-	1656 3060	1465 837
R25	sil.	nodule	sharp	-	1008	1244 941
R26	sil.	circular	sharp	-	1026	1183 793
R27	sil.	circular	sharp	-	1044	1156 797
R30/1	sil.	irregular	sharp	-	5941 3240	1293 591
R32	sil.	triangular	sharp	-	2160	1257 537
R33	sil.	circular	sharp	-	1782	954 444
R35	sil.	rounded	sharp	-	846	1061 686
R36	sil.	complex	sharp	-	2520 3780	602 774
3	cuspid	-	LB	-	9541 14401	319 161
R37	sil.	long	sharp	-	1458 3240	462 694
4	sil.	nodule	sharp	-	900	483 608
R38A	sil.	circular	sharp	-	1350	481 635
R38B	sil.	knotty	-	-	630	436 636
R39	sil.	nodule	sharp	-	882	742 160
R40A	sil.	nodule	sharp	-	450	451 267
R40B	sil.	nodule	sharp	-	468	457 252
R40C	sil.	nodule	sharp	-	522	468 235
R41	sil.	nodule	sharp	-	558	119 186
R42	sil.	nodule	sharp	-	540	48 206
M 16						
1	sil.	circular	sharp	near frag. 4	749	1383 736
2	sil.	circular	sharp	near frag. 4	1498	1398 931
3	cuspid	oval	LB	near frag. 4	963 1904	1005 1509
4	fragment	complex	mix	near ridge	25682	916 1307
5	cuspid	3-point	sharp	attached frag. 4	3210 6635	949 1478
6	cuspid	rounded	sharp	attached frag. 4	1819 2568	882 1203
7	cuspid	rounded	LB	attached frag. 4	1712 8132	1013 1152
M 17						
1	sil.	-	sharp	attached frag. ?	494 689	1572 4182
2	fragment	-	LB	near ridge	1950 3900	705 3720
3	cuspid	-	LB	isolated	715	2676 3910
4	fragment	-	LB	attached ridge ?	28603 29903	3353 3736
5	fragment	-	LB	attached ridge ?	10921 23402	3362 3019
6	cuspid	long w/ tail	LB	near frag. 5	1170 14301	3866 2817
7	sil.	circular	mix	isolated	1430 1690	972 2277
8	sil.	hook-shaped	sharp	near frag. 6	1170	3930 3177

TABLE 4—*Continued*

ID	Class	Shape	Edges	Location	Short & Long ^a dimensions (AU)	(X,Y) ^b position (pix)
9	cusp	-	LB	near cusp 10	325	3866 3564
10	cusp	-	LB	near cusp 9	650	3866 3564
11	cusp	rounded	LB	near cusps 9,10	845	4204 3900
12	sil.	edge-on	sharp	near ridge	1170 195	2022 3844
13	fragment	rounded	LB	isolated	16251 11246	1377 1550

^alinear sizes are determined using the distance estimates from Table 2.

^bThese are the pixel positions in the following images: j8rh02011_drz.fits (NGC 6530), j8rh04011_drz.fits (NGC 2467), j8rh05011_drz.fits (Pismis 24), j8rh06011_drz.fits (IC 1590), u57v0101r (IC 2944), u6dn3105m (M 16) and j8cw078b1i_drz.fits (M 17)

^cThe numbering scheme for these features follows Reipurth et al. (2003) except for a few fragments (whose numbers are not preceded by the letter R) that were not identified by them.

NOTE.—Class: “sil.” stands for silhouette; Shape: when a ‘-’ is seen in lieu of the shape of a cusp it is because the cusp is tear-shaped. Edges: “LB” stands for limb-brightened. If the edge is *not* LB then it can be sharp, fuzzy or a mix of both.

TABLE 5
SIZES OF PROPLYD AND PROPLYD-LIKE FEATURES.

Region	Distance (kpc)	Dark Sil. Size (AU)	Bright Cusps Chord (AU)	Comments
From the literature.				
Orion Nebula ^a	0.43	65-800	50-1700	<i>Bona fide</i> proplyds mostly with central stars
NGC 3372 ^b	2.3	3060	3750-6900	Several found. No central stars.
M 20 ^c	1.68	470?	1070	One found with disk, cusp and central star.
M 16 ^d	2	-	300-700	Some with central stars.
NGC 3603 ^e	6	-	6000	Several found.
M 8 ^f	1.8	-	615	One found with central star.
IC 2944	1.8	-	720-6400	Many silhouettes, some circular.
This work.				
NGC 2467	4.1	-	820-4500	Few found no central stars.
Pismis 24	2.5	2400	500-2100	One dark feature with halo, no star. Few bright found no central stars.
M 16	2.14	750-1500	See above.	Two found no central stars.
M 17	1.3	1170	325-845	Few cusps found no central stars. One disk with star; Fig.16.

^aBally et al. (2000); the largest cusp chords, ~ 1700 AU, are those of proplyd 244-440 (Henney & O'Dell 1999) and 181-826 (Bally et al. 2005).

^bSmith et al. (2003)

^cYusef-Zadeh et al. (2005)

^dHester et al. (1996); the associated stars are not in the middle of the cusps.

^eBrandner et al. (2000)

^fStecklum et al. (1998)